

LA-UR-18-30511

Approved for public release; distribution is unlimited.

Title: Sensitivity Analysis and Uncertainty Quantification Applied to the
Feynman Y and Sm2

Author(s): Clark, Alexander Rich

Intended for: Report

Issued: 2018-11-02

Disclaimer:

Los Alamos National Laboratory, an affirmative action/equal opportunity employer, is operated by the Los Alamos National Security, LLC for the National Nuclear Security Administration of the U.S. Department of Energy under contract DE-AC52-06NA25396. By approving this article, the publisher recognizes that the U.S. Government retains nonexclusive, royalty-free license to publish or reproduce the published form of this contribution, or to allow others to do so, for U.S. Government purposes. Los Alamos National Laboratory requests that the publisher identify this article as work performed under the auspices of the U.S. Department of Energy. Los Alamos National Laboratory strongly supports academic freedom and a researcher's right to publish; as an institution, however, the Laboratory does not endorse the viewpoint of a publication or guarantee its technical correctness.

Los Alamos

NATIONAL LABORATORY

memorandum

X-Computational Physics Division

Monte Carlo Methods, Codes, and Applications Group

Group XCP-3 MS F663

Los Alamos, New Mexico 87545

505-667-1920

To/MS: Distribution

From/MS: Alexander Clark / XCP-3, MS P363

Phone/Email: 505-667-4312/arclark@lanl.gov

Symbol: XCP-3:18-052(U)

Date: October 31, 2018

SUBJECT: (U) Sensitivity Analysis and Uncertainty Quantification Applied to the Feynman Y and Sm_2

Abstract

Neutron multiplicity counting (NMC) experiments are frequently used to perform non-destructive assay (NDA) of special nuclear material (SNM), but MCNP[®] code simulations of the counting distribution that were performed by Miller have revealed over-calibration in the value of the Pu-239 $\bar{\nu}$. Mattingly has demonstrated the procedure for deterministic calculations of the counting distribution moments and O'Brien implemented a first-order, adjoint-based sensitivity analysis (SA) methodology applied to the counting distribution moments. In this report, these techniques are used to apply SA/uncertainty quantification (UQ) to the Feynman Y and Sm_2 , which are ratios of the counting distribution moments. Sm_2 is less sensitive to the cross sections than Y and therefore has less variance due to covariance in the cross sections than Y .

The Feynman Y has historically been used to infer integral properties of SNM, such as neutron dispersion, neutron lifetime, and neutron multiplication. Sm_2 is a relatively new measure of the behavior of SNM that has not yet been used to infer integral properties of SNM, although measurements of Sm_2 for different source-detector distances have been compared to MCNP[®] code simulation by McSpaden. In this report, linear and quadratic models are fit to Sm_2 as a function of polyethylene reflector thickness and neutron multiplication and the observed trends are compared to those of Y to the same independent variables. Sm_2 is linear with respect to source and k_{eff} multiplication and quadratic with respect to polyethylene reflector thickness; therefore, these characteristics of an assembly of SNM may potentially be inferred using measurements of Sm_2 .

I Introduction

Neutron multiplicity counting (NMC) experiments are frequently used to perform non-destructive assay (NDA) of special nuclear material (SNM) [1]. A neutron multiplicity counter is used to accumulate the distribution of coincident multiplets of neutron counts for a given coincidence gate. The top portion of Fig. 1a depicts a detector pulse train that is segmented into sequential, equal-width coincidence gates, which are so called because neutron counts occurring within the same gate are considered to be coincident. The bottom part of Fig. 1a shows the accumulation of the frequency of multiplet neutron counts. Figure 1b was created by accumulating several multiplet neutron counts for a multiplicity counter counting a highly multiplying sphere of weapons-grade plutonium metal. The red line is a Poisson distribution with the same mean.

The NMC or counting distribution for independent neutron emissions, such as neutrons emitted from (α, n) reactions, is a Poisson distribution, where the variance and higher-order moments are all explicitly defined by the mean. In particular, the variance of a Poisson distribution is equal to its mean. Neutrons produced in fission-chain reactions, however, are emitted in bursts that are correlated in time. The counting distribution for fissionable material is therefore a generalized Poisson distribution, which requires higher-order moments to fully characterize.

MCNP[®] and Monte Carlo N-Particle[®] are registered trademarks owned by Los Alamos National Security, LLC, manager and operator of Los Alamos National Laboratory. Any third-party use of such registered marks should be properly attributed to Los Alamos National Security, LLC, including the use of the [®] designation as appropriate. Any questions regarding licensing, proper use, and/or proper attribution of Los Alamos National Security, LLC marks should be directed to trademarks@lanl.gov.

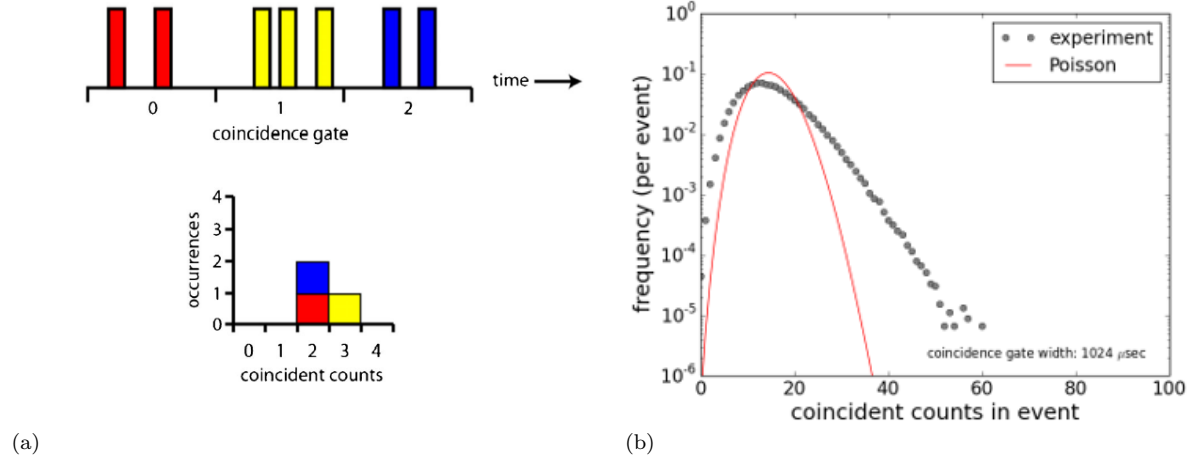


Figure 1: (a) Accumulation of the counting distribution [2]. (b) The counting distribution for a sphere of weapons-grade plutonium metal and a Poisson distribution with the same mean [3].

The Feynman Y and Sm_2 are both ratios of moments of the counting distribution. The Feynman Y variance-to-mean ratio

$$Y \equiv \frac{\sigma_n^2}{\bar{n}} - 1, \quad (1)$$

where \bar{n} and σ_n^2 are respectively the mean and variance of the counting distribution, is a measure of the deviation of the counting distribution from Poisson statistics and has historically been used to infer integral properties of SNM, such as neutron lifetime and neutron multiplication. Assay of SNM using Y requires that the detector response function be well-characterized for the assembly [3, 4].

The Sm_2 doubles-to-singles-squared ratio

$$Sm_2 \equiv \frac{D}{S^2}, \quad (2)$$

where S and D are respectively the first and second reduced-factorial moments of the counting distribution (often referred to as singles and doubles), is a relatively new metric used in NDA of SNM and is independent of the detector response function. For the same SNM assembly, two different neutron multiplicity counters or the same multiplicity counter at two different distances from the assembly will observe the same Sm_2 value. Simulations of NMC experiments used to compute Sm_2 will therefore not need to model the multiplicity counter, which removes a potential source of systematic error (i.e. uncertainty in the detector response function and/or uncertainty in the source-detector distance) between measured and simulated counting distribution moments [5, 6].

Miller found that MCNP[®] code simulations of NMC of a 4.5-kg sphere of alpha-phase, weapons-grade plutonium metal, a.k.a. the BeRP ball, consistently overpredicted the mean and variance of the counting distribution due to over-calibration of the Pu-239 $\bar{\nu}$ and he recommended a small scalar reduction in its value [2]. Evans used Cacuci's data assimilation (DA) methodology to perform an energy-dependent optimization of the Pu-239 $\bar{\nu}$ using 3D Denovo [7] simulations of gross neutron counting of the BeRP ball and he similarly recommended a reduction of one standard deviation in its value above 100 keV incident neutron energy and two standard deviations below 100 keV [8]. The ENDF/B-VII evaluators noted [9] that the value of the Pu-239 $\bar{\nu}$ was increased by more than two standard deviations above its previously evaluated value to match JEZEBEL critical experiments, which is consistent with the findings of Miller and Evans. I am currently investigating DA of cross sections (which collectively refers to cross sections and fission parameters such as the fission spectrum χ and moments of the fission multiplicity distribution $p(\nu)$) applied to NMC experiments to optimize cross sections such that the counting distribution moments are more accurately

simulated with reduced uncertainty. Performing this DA requires the sensitivity of the counting distribution moments to the cross sections as well as the variance in the counting distribution moments due to covariance in the cross sections, which may be computed using adjoint-based sensitivity analysis and first-order uncertainty quantification (SA/UQ), respectively. This SA/UQ methodology may also be applied to Y and Sm_2 and is the primary focus of this memo.

Muñoz-Cobo used a probabilistic description of the neutron population developed by Pål [10] and Bell [11] to derive the stochastic transport equation (STE), the solution of which is a probability generating function (PGF) [12]. The first moment of the PGF is the usual adjoint Boltzmann neutron transport equation (NTE), and higher-order moments are adjoint-like transport equations with the same adjoint transport operator but different, fixed adjoint source terms; consequently, standard transport solvers may be used to calculate these higher-order adjoint fluxes. Mattingly [3] used Muñoz-Cobo’s methodology to perform deterministic calculations of the counting distribution moments and O’Brien [13] demonstrated that first-order perturbation theory could be used to compute the sensitivity of the counting distribution moments to the cross sections using adjoint-based SA methods. The same methodologies may be used to compute Y and Sm_2 and their sensitivity to the cross sections because they are ratios of moments of the counting distribution.

The Feynman Y has historically been used to infer integral properties of SNM, such as neutron dispersion, neutron lifetime, and neutron multiplication [14, 15]. Sm_2 is a relatively new measure of the behavior of SNM that has not yet been used to infer integral properties of SNM, although measurements of Sm_2 for different source-detector distances have been compared to MCNP[®] code simulation [5, 6]. Sm_2 would be useful for NDA of SNM because it is independent of the detector response function. As a relatively simple starting point, the trend of Sm_2 as a function of polyethylene reflector thickness and neutron multiplication in the BeRP ball is contrasted with that of Y . Because Y is a function of the detector response function while Sm_2 is not, their respective trends differ significantly.

Two sets of novel results are presented in this memo: 1) The first application of SA/UQ to Y and Sm_2 and 2) analysis of trends in Y and Sm_2 as a function of polyethylene reflector thickness and neutron multiplication in the BeRP ball. Sections II.A and II.B provide a brief summary of the definition and use of Y and Sm_2 . Sections II.C and II.D summarize the perturbation theory-based SA methodology and derive the specific form of the sensitivity of the first and second counting distribution moments (a.k.a. detector response moments) to the cross sections. Section II.E defines the sensitivity of Y and Sm_2 to the cross sections in terms of the first- and second-moment detector response sensitivities. Section II.F describes how the variance in Y and Sm_2 due to covariance in the cross sections is computed using first-order propagation of uncertainty. Section II.G provides various definitions of neutron multiplication against which trends in Y and Sm_2 are observed.

Section III.A summarizes the first application of SA/UQ of Y and Sm_2 . Section III.B is a first look at the trends observed in fitting linear and quadratic models of Y and Sm_2 as a function of both polyethylene reflector thickness and neutron multiplication in the BeRP ball. Section IV provides a summary and recommendations. Sample PARTISN input decks are provided in Appendix A.

II SA/UQ methodology

II.A The Feynman Y

Y defined in Eq. (1) may be recast as

$$Y = \frac{R_2}{R_1}, \quad (3)$$

where R_1 is

$$R_1 \equiv \langle \psi_1^+, Q \rangle = \langle \psi, Q_1^+ \rangle \quad (4)$$

and R_2 is

$$R_2 \equiv \langle \psi, Q_2^+ \rangle + \langle S, Q_{2, sf}^+ \rangle. \quad (5)$$

S is the spontaneous fission rate density and spectrum of the forward intrinsic source,

$$S(\vec{r}, E) \equiv \frac{\chi_{sf}(E) F(\vec{r})}{4\pi}, \quad (6)$$

where χ_{sf} is the spontaneous fission neutron spectrum and F is the rate density at which spontaneous fissions occur, such that the forward, intrinsic source Q may be written as

$$Q(\vec{r}, E) \equiv \bar{\nu}_{sf} S(\vec{r}, E). \quad (7)$$

R_1 of Eq. (4) is the mean count rate of a detector and is equivalent to the mean of the NMC distribution (\bar{n} from Eq. (1)) and singles. R_1 is computed by solving the usual forward or adjoint NTE for the forward ψ or adjoint ψ_1^+ flux, respectively, by defining the adjoint source term Q_1^+ as the detector response function. Microscopic cross sections for reaction x and isotope j are denoted by $\sigma_{x,j}$ and the corresponding number density is denoted by N_j such that $\Sigma_{x,j} = N_j \sigma_{x,j}$ is the macroscopic cross section for reaction x and isotope j . For a multi-region assembly, all material properties, including N_j and all microscopic cross sections, are assumed to be constant in each region. N_j in different regions for the same isotope j may still have different values.

Muñoz-Cobo demonstrated that higher-order moments of the counting distribution may be computed by using the solution of the STE to derive higher-order adjoint NTEs [12]. The second-moment detector response R_2 of Eq. (5) is the variance in the counting distribution (in excess of the Poisson contribution) due to spontaneous and induced fission and is computed with the second-order adjoint source in Eq. (5),

$$Q_2^+(\vec{r}, E) \equiv \overline{\nu(\nu-1)}(E) \Sigma_f(E) I_1^2(\vec{r}), \quad (8)$$

which is the source for the second-order adjoint NTE

$$L^+ \psi_2^+ = Q_2^+. \quad (9)$$

The spontaneous fission, second-order adjoint source in Eq. (5) is

$$Q_{2, sf}^+(\vec{r}) \equiv \overline{\nu(\nu-1)}_{sf} I_{1, sf}^2(\vec{r}). \quad (10)$$

$\overline{\nu(\nu-1)}$ and $\overline{\nu(\nu-1)}_{sf}$ are the second factorial moments of the induced and spontaneous fission multiplicity distributions $p(\nu, E)$ and $p_{sf}(\nu)$, respectively, with $\bar{\nu}$ and $\bar{\nu}_{sf}$ as their respective means. The order- k factorial moments of $p(\nu, E)$ and $p_{sf}(\nu)$ are

$$\overline{\nu(\nu-1)\dots(\nu-k+1)}(E) \equiv \sum_{\nu=0}^{\nu_{max}} \nu(\nu-1)\dots(\nu-k+1) p(\nu, E), \quad (11)$$

$$\overline{\nu(\nu-1)\dots(\nu-k+1)}_{sf} \equiv \sum_{\nu=0}^{\nu_{max}} \nu(\nu-1)\dots(\nu-k+1) p_{sf}(\nu) \quad (12)$$

respectively, where ν represents the number of neutrons emitted per fission. Note that $p(\nu, E)$ and its moments are functions of incident neutron energy whereas $p_{sf}(\nu)$ is independent of incident neutron energy.

The “importance” of induced and spontaneous fission neutrons to the mean count rate are respectively

$$I_1(\vec{r}) \equiv \int d\Omega' \int dE' \frac{\chi(E')}{4\pi} \psi_1^+(\vec{r}, \hat{\Omega}', E'), \quad (13)$$

$$I_{1,sf}(\vec{r}) \equiv \int d\Omega' \int dE' \frac{\chi_{sf}(E')}{4\pi} \psi_1^+(\vec{r}, \hat{\Omega}', E'), \quad (14)$$

where χ is the induced fission neutron spectrum. Note that χ is the distribution of energies for neutrons emerging from induced fission and is here approximated as independent of incident neutron energy. In the present notation, it is assumed that spontaneous and induced fission each only occur in one isotope. Moments of $p(\nu)$ and $p_{sf}(\nu)$, χ , χ_{sf} , and Σ_f therefore do not have an isotope index.

For a Poisson-distributed process where neutron emissions are independent of one another, the variance of the counting distribution is simply equal to the mean and R_2 is zero. The variance in a counting distribution accumulated by counting SNM will, however, be greater than the mean because fission chain reactions are not independent of one another. Mattingly’s deterministic method [3] can be used to calculate Y because it may be expressed in terms of R_1 and R_2 .

II.B Sm₂

Sm₂ defined in Eq. (2) may also be recast in terms of R_1 and R_2 . Singles is identical to the mean count rate R_1 and both R_2 and doubles are related to the variance of the counting distribution. R_2 is the second factorial moment of the counting distribution $C(n)$ while doubles is the reduced-factorial moment of $C(n)$. An order- k factorial and reduced-factorial moment of $C(n)$ may respectively be defined as

$$\overline{n(n-1) \dots (n-k+1)} \equiv \sum_{n=1}^N n(n-1) \dots (n-k+1) C(n), \quad (15)$$

$$\overline{n(n-1) \dots (n-k+1)}_r \equiv \frac{1}{k!} \sum_{n=1}^N n(n-1) \dots (n-k+1) C(n), \quad (16)$$

where the difference between Eq. (15) and Eq. (16) is the normalization factor $\frac{1}{k!}$. This relationship between factorial- and reduced-factorial moments means that doubles and R_2 have the simple relationship

$$D = \frac{1}{2} R_2, \quad (17)$$

and Eq. (2) may be expressed as

$$\text{Sm}_2 = \frac{1}{2} \frac{R_2}{R_1^2}. \quad (18)$$

Thus, Mattingly’s deterministic method [3] can also be used to calculate Sm₂.

Sm₂ is independent of the detector response because R_1 and R_2 are a linear and quadratic function of the detector response function, respectively. R_1 in Eq. (4) is the inner product of the forward flux and the detector response function itself. The second-moment adjoint source terms (Eqs. (8) and (10)) used to compute R_2 in Eq. (5) are computed with the square of I_1 and $I_{1,sf}$, respectively, which means that the source terms contribute as the square of the detector response function. For the same assembly, counting distributions accumulated by different neutron

multiplicity counters or the same multiplicity counter at different distances from the assembly will yield the same Sm_2 values. This property is particularly useful when performing simulations of NMC experiments because the multiplicity counter does not need to be modeled. McSpaden demonstrated that Sm_2 values computed via MCNP® code simulations of the BeRP ball counted by the MC-15 neutron multiplicity counter agree with experimental values and are invariant with respect to source-detector distance [6]. With the need for detailed detector models in simulations obviated, a potential source for systematic errors between simulation and experiment is ameliorated.

II.C Sensitivity analysis of the mean count rate

The forward and adjoint NTE may be discretized in energy via the multigroup approximation [16],

$$f_g = \frac{\int_{\Delta E_g} dE W(E) f(E)}{\int_{\Delta E_g} dE W(E)}, g = 1, \dots, G, \quad (19)$$

where the cross sections, fluxes, and sources are averaged over a small energy interval ΔE_g with an averaging function $W(E)$. Multigroup cross sections and $p(\nu, E)$ moments may be obtained by choosing $W(E)$ to be the forward, scalar flux. Multigroup fluxes, sources, and fission spectrum may be obtained by setting $W(E)$ to unity.

With the multigroup approximation, the sensitivity of R_1 to a cross section (or fission parameter) α for isotope j at group g using first-order perturbation theory as described by O'Brien may be expressed as [13]

$$\frac{\partial R_1}{\partial \alpha_{j,g}} = \left\langle \frac{\partial Q_1^+}{\partial \alpha_{j,g}}, \psi \right\rangle + \left\langle \psi_1^+, \frac{\partial Q}{\partial \alpha_{j,g}} - \frac{\partial L}{\partial \alpha_{j,g}} \psi \right\rangle, \quad (20)$$

where the inner product is defined as

$$\langle f, h \rangle \equiv \int d^3r \int d\Omega \sum_{g'=1}^G f_{g'}(\vec{r}, \hat{\Omega}) h_{g'}(\vec{r}, \hat{\Omega}). \quad (21)$$

The magnitude of the absolute sensitivity defined in Eq. (20) can vary greatly with respect to cross section type and energy group, so it is useful to define a relative sensitivity that is scaled by the cross section and response values themselves,

$$S_{R_1, \alpha_{j,g}} = \frac{\alpha_{j,g}}{R_1} \frac{\partial R_1}{\partial \alpha_{j,g}}. \quad (22)$$

It will always be clear from context whether S refers to the spontaneous fission rate density and spectrum of Eq. (6) or a relative sensitivity, such as that defined in Eq. (22). The relative sensitivity is used to approximate a linear relationship between a small change in the cross section and a corresponding change in R_1 . Table 1 summarizes the analytic form of the relative sensitivity of R_1 to specific cross sections. The sensitivity of R_1 to the cross sections may be calculated by solving for forward and adjoint angular fluxes and flux moments and computing the sums and integrals given in Table 1 for a specific cross section.

Table 1: Relative sensitivity of R_1 to the set of cross sections $\chi_g, \bar{\nu}_g, \sigma_{f,g}, \sigma_{s,j,g}, \sigma_{c,j,g}$. An analogous table is given by Favorite in Table 1 in the SENSMSG manual for the indirect effect of the sensitivity of neutron leakage to the cross sections [17]. The sensitivities given by Favorite are defined using a chi matrix (fission neutron spectrum as a function of incident neutron energy) while the sensitivities given here are defined using a chi vector (fission neutron spectrum independent of incident neutron energy) [16]. $S_{R_1, \sigma_{s,j,g}}$ is the sum of Favorite's sensitivity of R_1 to $\sigma_{s,j,g \rightarrow g'}^m$ over all outgoing energy groups g' and Legendre polynomial expansion moments m .

$S_{R_1, \chi_g}, (a)$	$\frac{1}{R_1} \int d^3r \chi_g \phi_{1,g}^{+,0}(\vec{r}) \sum_{g'=1}^G \bar{\nu}_{\Sigma_{f,g'}} \phi_{g'}^0(\vec{r})$
$S_{R_1, \bar{\nu}_g}$	$\frac{1}{R_1} \int d^3r I_1(\vec{r}) \bar{\nu}_{\Sigma_{f,g}} \phi_g^0(\vec{r})$
$S_{R_1, \sigma_{f,g}}$	$\frac{1}{R_1} \left[\int d^3r I_1(\vec{r}) \bar{\nu}_{\Sigma_{f,g}} \phi_g^0(\vec{r}) - \int d^3r \int d\Omega \Sigma_{f,g} \psi_g(\vec{r}, \hat{\Omega}) \psi_{1,g}^+(\vec{r}, \hat{\Omega}) \right]$
$S_{R_1, \sigma_{s,j,g}}$	$\frac{1}{R_1} \left[\int d^3r \sum_{m=0}^M \phi_g^m(\vec{r}) \sum_{g'=1}^G \Sigma_{s,j,g \rightarrow g'}^m \phi_{1,g'}^{+,m}(\vec{r}) - \int d^3r \int d\Omega \psi_g(\vec{r}, \hat{\Omega}) \Sigma_{s,j,g}^0 \psi_{1,g}^+(\vec{r}, \hat{\Omega}) \right]$
$S_{R_1, \sigma_{c,j,g}}$	$-\frac{1}{R_1} \int d^3r \int d\Omega \Sigma_{c,j,g} \psi_g(\vec{r}, \hat{\Omega}) \psi_{1,g}^+(\vec{r}, \hat{\Omega})$
(a) This definition is for an unconstrained sensitivity. See [18] for relationship between unconstrained and constrained sensitivities.	

The sensitivities given in Table 1 are defined in terms of forward and adjoint inner products for angular fluxes as well as Legendre polynomial expansion moments of the angular fluxes for a one-dimensional (spherical) geometry. The scatter cross section is also given in terms of its Legendre polynomial expansion moments. The form of the order- m forward flux, adjoint flux, and scatter cross section moments are respectively defined as [16]

$$\phi_g^m(\vec{r}) = \frac{1}{2} \int_{-1}^1 d\mu P^m(\mu) \psi_g(\vec{r}, \mu), \quad (23)$$

$$\phi_{k,g}^{+,m}(\vec{r}) = \frac{1}{2} \int_{-1}^1 d\mu P^m(\mu) \psi_{k,g}^+(\vec{r}, \mu), k = 1, 2, \quad (24)$$

$$\Sigma_{s,j,g \rightarrow g'}^m = \frac{2m+1}{2} \int_{-1}^1 d\mu P^m(\mu) \int_{-1}^1 d\mu' P^m(\mu') \Sigma_{s,j,g \rightarrow g'}(\mu \cdot \mu'), \quad (25)$$

$$\Sigma_{s,j,g}^m = \sum_{g'=1}^G \Sigma_{s,j,g \rightarrow g'}^m, \quad (26)$$

where P^m is a Legendre polynomial of order m and M is an arbitrarily chosen maximum Legendre polynomial order. $m = 0$ denotes an isotropic flux or scatter cross section while $m > 0$ denotes increasing orders of anisotropy. The inclusion of the $2m+1$ normalization factor in Eq. (25) is consistent with the scatter cross section moments generated

by SCALE, from which the cross sections and their covariances are obtained [19].

Inner products between the forward and adjoint flux moments must reflect the fact that the adjoint angular flux is defined for directions that are opposite of the forward angular flux. Favorite distinguished between computational moments, which are calculated by transport solvers and defined by Eqs. (23), (24), and (25), and inner product moments, which account for the reversal in the adjoint flux direction [20]. Irrespective of geometry, this amounts to a simple correction factor that is positive for the zeroeth and even moments and negative for odd moments. The relationship between computational and inner product moments for the forward and adjoint flux moments is then

$${}^{IP}\phi_g^m = (-1)^m \phi_g^m, \quad (27)$$

$${}^{IP}\phi_{k,g}^{+,m} = (-1)^m \phi_{k,g}^{+,m}, k = 1, 2, \quad (28)$$

such that the inner product between the forward and adjoint flux moments is

$$\langle {}^{IP}\phi_g^m, \phi_{k,g}^{+,m} \rangle = \langle {}^{IP}\phi_{k,g}^{+,m}, \phi_g^m \rangle = \langle (-1)^m \phi_g^m, \phi_{k,g}^{+,m} \rangle, k = 1, 2. \quad (29)$$

II.D Sensitivity analysis of the second-moment detector response

First-order perturbation theory may also be used to derive the sensitivity of the second-moment detector response R_2 to a cross section α for isotope j at group g [13],

$$\begin{aligned} \frac{\partial R_2}{\partial \alpha_{j,g}} = & \left\langle \psi_2^+, \frac{\partial Q}{\partial \alpha_{j,g}} - \frac{\partial L}{\partial \alpha_{j,g}} \psi \right\rangle + 2 \left\langle \Phi_1 + \Phi_{1,sf}, \frac{\partial Q_1^+}{\partial \alpha_{j,g}} - \frac{\partial L^+}{\partial \alpha_{j,g}} \psi_1^+ \right\rangle + \\ & \left\langle \frac{\partial Q_2^+}{\partial \beta_g}, \psi \right\rangle + \left\langle \frac{\partial Q_{2,sf}^+}{\partial \beta_g}, S \right\rangle + \left\langle Q_{2,sf}^+, \frac{\partial S}{\partial \alpha_{j,g}} \right\rangle, \end{aligned} \quad (30)$$

where $\beta_g = \{\overline{\nu(\nu-1)}_g, \overline{\nu(\nu-1)}_{sf}, \sigma_{f,g}, \chi_g, \chi_{g,sf}\}$ is the subset of $\alpha_{j,g}$ that appears explicitly in the adjoint source terms in Eqs. (8) and (10).

Two new forward fluxes, Φ_1 and $\Phi_{1,sf}$, have been introduced in Eq. (30) that represent the flux of neutrons that contribute to R_2 and are obtained by solving special forward transport equations that satisfy [13]

$$L\Phi_1 = I_1 Q_{f1}, \quad (31)$$

$$L\Phi_{1,sf} = I_{1,sf} Q_{f1,sf}, \quad (32)$$

where the new forward source terms are

$$Q_{g,f1}(\vec{r}) = \chi_g \sum_{g'=1}^G \overline{\nu(\nu-1)}_{\Sigma_{f,g'}} \phi_{g'}^0(\vec{r}), \quad (33)$$

$$Q_{g,f1,sf}(\vec{r}) = \chi_{g,sf} \sum_{g'=1}^G \overline{\nu(\nu-1)}_{S_{g'}} S_{g'}^0(\vec{r}). \quad (34)$$

The relative sensitivity of R_2 to a cross section has the same form and interpretation as that for R_1 ,

$$S_{R_2, \alpha_{j,g}} = \frac{\alpha_{j,g}}{R_2} \frac{\partial R_2}{\partial \alpha_{j,g}}. \quad (35)$$

Table 2 summarizes the analytic form of the relative sensitivity vectors of R_2 to the transport parameters at group g . The new forward fluxes defined by Eqs. (31) and (32) are added for convenience,

$$\Phi = \Phi_1 + \Phi_{1,sf}. \quad (36)$$

The sensitivity of R_2 to each cross section is computed in the same way as the sensitivity of R_1 to each cross section is (see Sec. II.C).

Table 2: Relative sensitivity of R_2 to the set of cross sections $\chi_g, \bar{\nu}_g, \overline{\nu(\nu-1)}_g, \sigma_{f,g}, \sigma_{s,j,g}, \sigma_{c,j,g}$.

$S_{R_2, \chi_g}, (a)$	$\frac{1}{R_2} \left[\int d^3r \chi_g \phi_{2,g}^{+,0}(\vec{r}) \sum_{g'=1}^G \bar{\nu} \Sigma_{f,g'} \phi_{g'}^0(\vec{r}) + 2 \int d^3r \chi_g \phi_{1,g}^{+,0}(\vec{r}) \sum_{g'=1}^G \bar{\nu} \Sigma_{f,g'} \varphi_{g'}^0(\vec{r}) + \right. \\ \left. 2 \int d^3r \chi_g \phi_{1,g}^{+,0}(\vec{r}) I_1(\vec{r}) \sum_{g'=1}^G \overline{\nu(\nu-1)} \Sigma_{f,g'} \phi_{g'}^0(\vec{r}) \right]$
$S_{R_2, \bar{\nu}_g}$	$\frac{1}{R_2} \left[\int d^3r I_2(\vec{r}) \bar{\nu} \Sigma_{f,g} \phi_g^0(\vec{r}) + 2 \int d^3r I_1(\vec{r}) \bar{\nu} \Sigma_{f,g} \varphi_g^0(\vec{r}) \right]$
$S_{R_2, \overline{\nu(\nu-1)}_g}$	$\frac{1}{R_2} \left[\int d^3r \overline{\nu(\nu-1)} \Sigma_{f,g} I_1^2(\vec{r}) \phi_g^0(\vec{r}) \right]$
$S_{R_2, \sigma_{f,g}}$	$\frac{1}{R_2} \left[\int d^3r I_2(\vec{r}) \bar{\nu} \Sigma_{f,g} \phi_g^0(\vec{r}) - \int d^3r \int d\Omega \Sigma_{f,g} \psi_{2,g}^+(\vec{r}, \hat{\Omega}) \psi_g(\vec{r}, \hat{\Omega}) + \right. \\ \left. 2 \int d^3r I_1(\vec{r}) \bar{\nu} \Sigma_{f,g} \varphi_g^0(\vec{r}) - 2 \int d^3r \int d\Omega \Sigma_{f,g} \psi_{1,g}^+(\vec{r}, \hat{\Omega}) \Phi_g(\vec{r}, \hat{\Omega}) + \right. \\ \left. \int d^3r I_1^2(\vec{r}) \overline{\nu(\nu-1)} \Sigma_{f,g} \phi_g^0(\vec{r}) \right]$
$S_{R_2, \sigma_{s,j,g}}, (b)$	$\frac{1}{R_2} \left[\int d^3r \sum_{m=0}^M \phi_g^m(\vec{r}) \sum_{g'=1}^G \Sigma_{s,j,g \rightarrow g'}^m \phi_{2,g'}^{+,m}(\vec{r}) - \int d^3r \int d\Omega \psi_g(\vec{r}, \hat{\Omega}) \Sigma_{s,j,g}^0 \psi_{2,g}^+(\vec{r}, \hat{\Omega}) + \right. \\ \left. 2 \int d^3r \sum_{m=0}^M \varphi_g^m(\vec{r}) \sum_{g'=1}^G \Sigma_{s,j,g \rightarrow g'}^m \phi_{1,g'}^{+,m}(\vec{r}) - 2 \int d^3r \int d\Omega \Phi_g(\vec{r}, \hat{\Omega}) \Sigma_{s,j,g}^0 \psi_{1,g}^+(\vec{r}, \hat{\Omega}) \right]$
$S_{R_2, \sigma_{c,j,g}}$	$-\frac{1}{R_2} \left[\int d^3r \int d\Omega \psi_{2,g}^+(\vec{r}, \hat{\Omega}) \Sigma_{c,j,g} \psi_g(\vec{r}, \hat{\Omega}) + 2 \int d^3r \int d\Omega \psi_{1,g}^+(\vec{r}, \hat{\Omega}) \Sigma_{c,j,g} \varphi_g(\vec{r}, \hat{\Omega}) \right]$

(a) This definition is for an unconstrained sensitivity. See [18] for relationship between unconstrained and constrained sensitivities.

(b) This is the sensitivity of R_2 to all neutron scatter reactions from group g to any other group for all Legendre polynomial expansion orders.

The second-moment forward flux Φ is also given in terms of Legendre polynomial expansion moments and is

discretized via the multigroup approximation,

$$\varphi_g^m(\vec{r}) = \frac{1}{2} \int_{-1}^1 d\mu P^m(\mu) \Phi_g(\vec{r}, \mu). \quad (37)$$

The “importance” of induced fission neutrons to the second-moment detector response I_2 in Table 2 is defined as

$$I_2(\vec{r}) \equiv \sum_{g'=1}^G \chi_{g'} \phi_{2,g'}^{+,0}(\vec{r}), \quad (38)$$

which is similar to the definition of I_1 in Eq. (13).

The first two terms in Eq. (30) contain $\bar{\nu}$ in the forward and adjoint transport operators, respectively, and the third term contains $\bar{\nu}(\bar{\nu} - 1)$ in Q_2^+ . Because $\bar{\nu}$ and $\bar{\nu}(\bar{\nu} - 1)$ are treated as independent parameters, $\frac{\partial Q_2^+}{\partial \bar{\nu}_g} = 0$ in the third term; therefore, $S_{R_2, \bar{\nu}_g}$ only has a contribution from the first two terms. $\bar{\nu}(\bar{\nu} - 1)$ only appears in Q_{2g}^+ and so $S_{R_2, \bar{\nu}(\bar{\nu}-1)_g}$ only has a contribution from the third term.

II.E Sensitivity analysis of the Feynman Y and Sm_2

The relative sensitivity of Y to a cross section is a linear combination of the relative sensitivities of R_1 and R_2 to that cross section, i.e.,

$$S_{Y, \alpha_{j,g}} = S_{R_2, \alpha_{j,g}} - S_{R_1, \alpha_{j,g}}. \quad (39)$$

The relative sensitivity of Sm_2 to a cross section may be similarly expressed as

$$S_{\text{Sm}_2, \alpha_{j,g}} = S_{R_2, \alpha_{j,g}} - 2S_{R_1, \alpha_{j,g}}, \quad (40)$$

where the factor of 2 in Eq. (40) is due to R_1 being squared in the denominator of Eq. (18).

II.F Uncertainty quantification

The variance in Y and Sm_2 due to covariance in the cross sections and fission parameters may be estimated with the usual formula for first-order propagation of uncertainty,

$$\text{var}(f) = \mathbf{S}_{f, \alpha}^T \text{cov}(\alpha, \alpha) \mathbf{S}_{f, \alpha}, f = Y, \text{Sm}_2. \quad (41)$$

Let X be the number of cross sections, J be the number of isotopes, G be the number of energy groups, and T be the product of X , J , and G . Then $\mathbf{s}_{f, \alpha}$ is a $T \times 1$ vector of sensitivities whose elements are $S_{f, \alpha_{j,g}}$ and $\text{cov}(\alpha, \alpha)$ is a $T \times T$ matrix of covariances between each cross section for each isotope and energy group. Note that there may be covariance between different isotopes (e.g. Pu-239 fission to Pu-240 fission), cross sections (e.g. the scatter and fission cross sections), and energy groups of the same cross section. The uncertainty in Y and Sm_2 is simply the square root of Eq. (41).

II.G Neutron multiplication definitions

The neutron multiplication of an assembly of material refers to the number of neutrons produced per source neutron. A material in which induced fissions or (n,xn) reactions for $x > 1$ do not occur will have a neutron multiplication of 1 by definition, while a material in which these events may occur will have a neutron multiplication greater than 1. Spontaneous fission events have an intrinsic multiplicity defined by a material's $p(\nu)_{sf}$ distribution, but in the absence of induced fission or (n,xn) reactions for $x > 1$, the neutron multiplication of the assembly is still unity. Spontaneous fission events occur independent of a source neutron and therefore are not included in the definition of neutron multiplication, although neutrons emitted from spontaneous fission may still act as source neutrons.

One way to define neutron multiplication is in terms of neutron leakage from the system, i.e.,

$$M_L \equiv \frac{\text{rate of neutron leakage}}{\text{rate of source neutron emission}}. \quad (42)$$

Leakage multiplication describes the total number of neutrons produced by the assembly that leave the system (and are thus available for detection) per source neutron. For a static, subcritical assembly, the rate of source neutron emission will remain unchanged with the addition of reflector material, while the rate of neutron leakage may vary.

Another way to define neutron multiplication is in terms of the production of neutrons in the assembly, i.e.,

$$M_S \equiv \frac{\text{rate of source neutron emission} + \text{rate of neutron production}}{\text{rate of source neutron emission}}. \quad (43)$$

Source multiplication describes the total number of neutrons produced by the assembly (not only those that escape the assembly) per source neutron. As with the leakage multiplication, as reflector material is added or removed, the rate of source neutron production will not vary, but the rate of neutron production will change.

A third way to define neutron multiplication is in terms of the effective multiplication factor k_{eff} , i.e.,

$$M_{k_{\text{eff}}} \equiv \frac{1}{1 - k_{\text{eff}}}, \quad (44)$$

where

$$k_{\text{eff}} \equiv \frac{\text{fission neutron production rate}}{\text{fission neutron loss due to leakage and absorption rate}}. \quad (45)$$

k_{eff} is the largest eigenvalue of the homogeneous NTE (i.e. the NTE for a critical assembly without an intrinsic source), where the corresponding eigenvector is the fundamental flux mode, which persists longer in time than higher-order flux modes. While the leakage and source multiplication are defined for a subcritical assembly with a fixed source, k_{eff} multiplication is defined either in the absence of a fixed source or with the assumption that the spatial and spectral fixed source distribution is identical to that of the induced fission source. It is also only a valid relationship for assemblies that are close to critical.

III Results and analysis

III.A PARTISN simulations of an NMC experiment

One-dimensional (spherical), 44-group PARTISN simulations of the nPod neutron multiplicity counter counting the BeRP ball in bare and polyethylene-reflected configurations were used to compute Y and Sm_2 , their sensitivity

to the cross sections, and their variance due to covariance in the cross sections. Figure 2 illustrates the corresponding NMC experiment [2]. The PARTISN simulations were performed using 256 discrete ordinates, order-5 Legendre polynomial expansion of the scatter cross section, 10^{-6} convergence tolerance, and a uniform spatial mesh cell thickness of 0.01 cm in the plutonium and polyethylene. The material compositions are given in Table 3 and the problem geometry is given in Table 4.

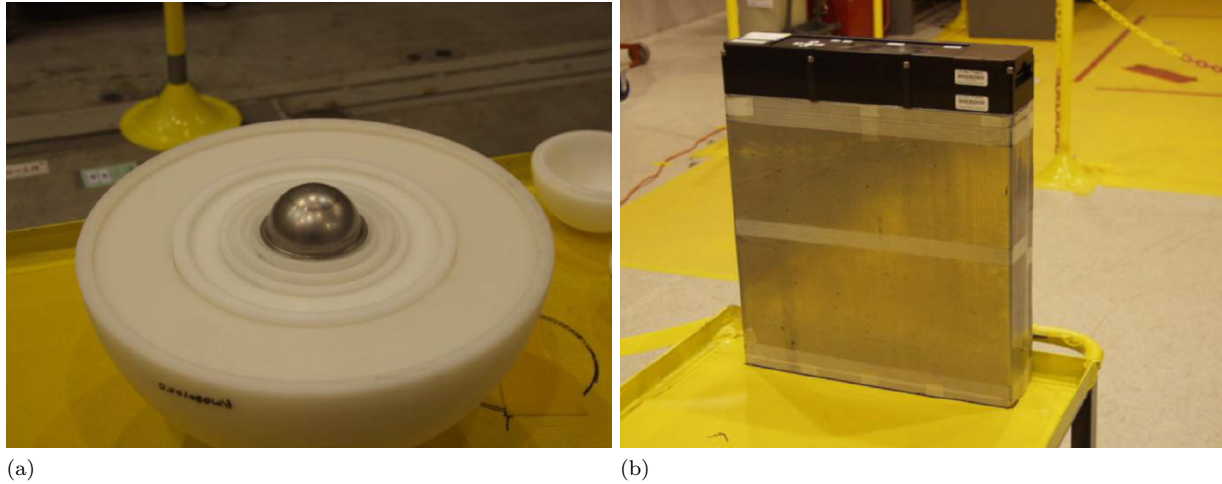


Figure 2: Setup of the NMC experiment. (a) A 4.5-kg sphere of weapons-grade, alpha-phase plutonium metal (a.k.a. the BeRP ball) nested in polyethylene reflectors. (b) The nPod neutron multiplicity counter, which is a polyethylene-moderated array of 15 He-3 proportional counters [2].

Table 3: Number density of each isotope in each material.

Material	Isotope	Number density ($\frac{\text{atom}}{\text{b cm}}$)
plutonium	Pu-239	4.605952×10^{-2}
	Pu-240	2.905037×10^{-3}
polyethylene	H-1	8.098822×10^{-2}
	C-12	4.040160×10^{-2}

Table 4: The number of spatial cells in and the outer radius of the bare and polyethylene-reflected BeRP ball configurations.

Reflector thickness (cm)	Cells in plutonium	Cells in polyethylene	Outer radius (cm)
0	379	0	3.794
1.3	379	127	5.064
2.5	379	254	6.334
3.8	379	381	7.604
7.6	379	762	11.414
15.2	379	1524	19.034

The set of 44-group cross sections included in the SA/UQ are those given in the caption for Table 2 for Pu-239 and H-1. Pu-240 is not included in the SA/UQ because it primarily acts as the spontaneous fission source that drives induced fission in Pu-239, while C-12 is not included in the SA/UQ because its contribution is negligibly small. The 44-group cross sections and their covariance data were obtained from the ENDF/B-VII.1 cross section library included with the SCALE code package [19].

Figure 3a is the relative sensitivity of Y to the Pu-239 $\bar{\nu}$ for the bare and 3.8-cm polyethylene-reflected BeRP ball configurations. Figure 3b is an analogous plot for Sm_2 . The sensitivity of Y and Sm_2 to the Pu-239 $\bar{\nu}$ are given because $\bar{\nu}$ has the greatest influence on the counting distribution moments.

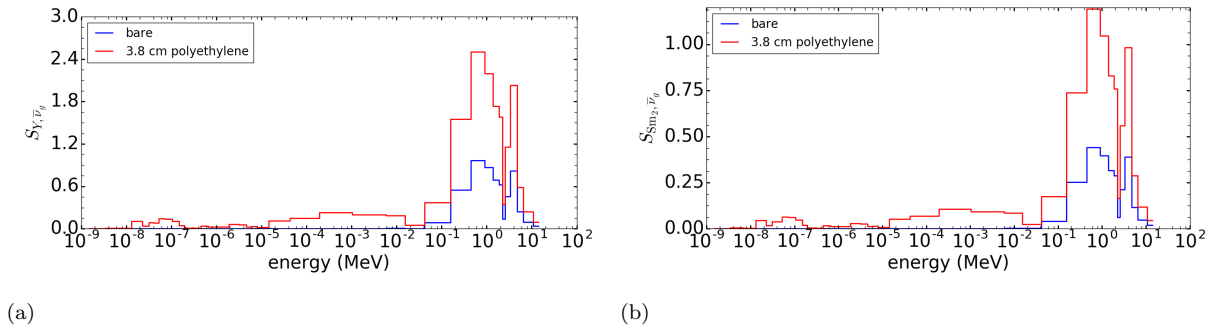


Figure 3: Relative sensitivity of (a) Y and (b) Sm_2 to the Pu-239 $\bar{\nu}$ for the bare and 3.8-cm polyethylene-reflected BeRP ball cases.

Y is more sensitive to $\bar{\nu}$ than Sm_2 for the bare and reflected configurations. An increase in $\bar{\nu}$ will increase both R_1 and R_2 because more neutrons will be emitted per induced fission in Pu-239. R_2 will increase more than R_1 because the system will emit larger bursts of neutrons that are correlated in time, which contribute more to the variance of the counting distribution (in excess of the Poisson contribution) than to the mean (which is entirely the Poisson contribution). Sm_2 is the ratio of R_2 to R_1 squared (see Eq. (18)), which means that it will increase more

slowly with $\bar{\nu}$ than will Y .

The sensitivity of Y and Sm_2 to $\bar{\nu}$ both have the largest magnitude in the fast energy groups, which indicates that changes in the fast group $\bar{\nu}$ will have the greatest effect on Y and Sm_2 . Additionally, the magnitude of the sensitivities increases significantly from the bare to reflected cases. In particular, the reflected case is sensitive to neutrons at all energies, while the bare case is sensitive to fast neutrons only. Neutrons that would otherwise escape the BeRP ball may instead be reflected and slowed down by the polyethylene, resulting in a greater number of neutrons available in the plutonium at lower energies, at which neutrons are most likely to induce fission. Y and Sm_2 are therefore more highly influenced by changes in $\bar{\nu}$ in the reflected case than in the bare case.

Figure 4a shows the relative sensitivity totals of Y to all of the cross sections for the bare and 3.8-cm polyethylene-reflected BeRP ball configurations. Figure 4b is an analogous plot for Sm_2 . The totals are the sum of the sensitivities over group and are useful for comparing the effect of a change in each of the cross sections on Y and Sm_2 .

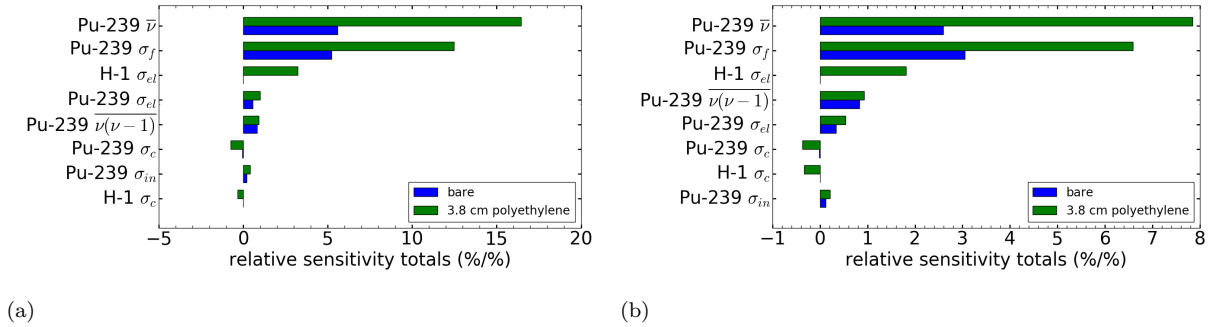


Figure 4: Relative sensitivity totals of (a) Y and (b) Sm_2 to the cross sections for the bare and 3.8-cm polyethylene-reflected BeRP ball cases.

The most influential cross sections on Y and Sm_2 are $\bar{\nu}$ and σ_f because they describe the number of neutrons emitted per fission and the probability that a fission will occur, respectively, which directly impact the number of neutrons produced by the assembly. The capture cross section has a negative sensitivity total while the other cross sections have a positive sensitivity total. This means that increasing the capture cross sections will decrease Y and Sm_2 while increasing the other cross sections will increase Y and Sm_2 . The sensitivity total of $\nu(\nu-1)$ is small compared to the other sensitivity totals, particularly $\bar{\nu}$. Fission chains in highly multiplying material (such as the BeRP ball) tend to be hundreds of generations long, which means that the number of neutrons emitted from the BeRP ball is driven primarily by the number of neutron generations, which is more greatly affected by the mean of $p(\nu, E)$ than by its dispersion.

Figure 5a is a plot of the measured [2] and simulated Feynman Y values for each BeRP ball configuration. The uncertainty in the simulated Y is due only to the covariance in the cross sections. The uncertainty in the measured Y is due only to the random nature of neutron counting and is too small to see on the plot. Figure 5b is an analogous plot of Sm_2 .

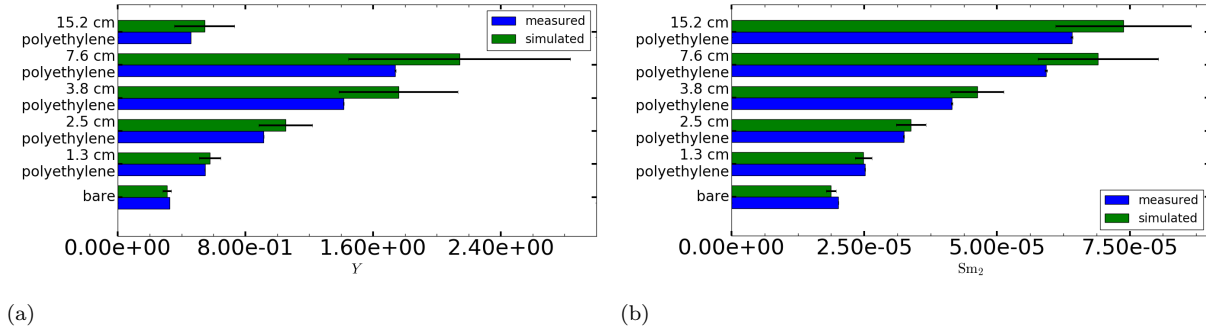


Figure 5: Y (a) and Sm_2 (a) values for the bare and all polyethylene-reflected BeRP ball cases. Uncertainty in the simulated values is due only to covariance in the cross sections.

Because Sm_2 is less sensitive to the cross sections than Y , it also has less variance (relative to its respective response value) due to covariance in the same cross sections. The measured and simulated Y become increasingly dissimilar as more reflector material is added, and a similar trend is observed in Sm_2 . As discussed in Section I, the same trend was observed by Miller [2] and Evans [8] in the counting distribution moments and found to be caused primarily by over-calibration in the Pu-239 $\bar{\nu}$. As previously discussed, an increase in $\bar{\nu}$ will increase both R_1 and R_2 , with R_2 increasing at a rate faster than R_1 , which will lead to an increase in Y and Sm_2 . Y and Sm_2 are more sensitive to $\bar{\nu}$ in the reflected case than the bare, so the effect of a change in $\bar{\nu}$ is amplified as polyethylene is added.

Y peaks at 7.6 cm of polyethylene reflector because it is a function of the detector response, which depends on neutron leakage. As polyethylene is added to the BeRP ball, neutrons are moderated down to energies at which fissions are more likely to occur and are reflected back into the plutonium metal. With enough polyethylene, the probability that neutrons are parasitically captured becomes comparable to the probability that neutrons will leave the system. The rise and fall of Y as a function of polyethylene reflector thickness is indicative of the competition between an increase in the number of neutrons produced by the assembly and the probability that neutrons are parasitically captured or moderated down to energies below which the nPod is sensitive. Sm_2 is insensitive to the detector response and therefore monotonically increases with respect to reflector thickness.

III.B Fitting the Feynman Y and Sm_2 vs reflector thickness and neutron multiplication

One-dimensional (spherical), 44-group PARTISN simulations of gross neutron counting experiments of the nPod neutron multiplicity counter counting the BeRP ball in bare and polyethylene-reflected configurations were used to compute source and leakage multiplication. k_{eff} -eigenvalue PARTISN simulations of the BeRP ball were used to compute k_{eff} multiplication. The same PARTISN solver options, materials, and geometry used in Sec. III.A were used for these calculations. Figure 6 is a plot of source, k_{eff} , and leakage multiplication as a function of polyethylene reflector thickness.

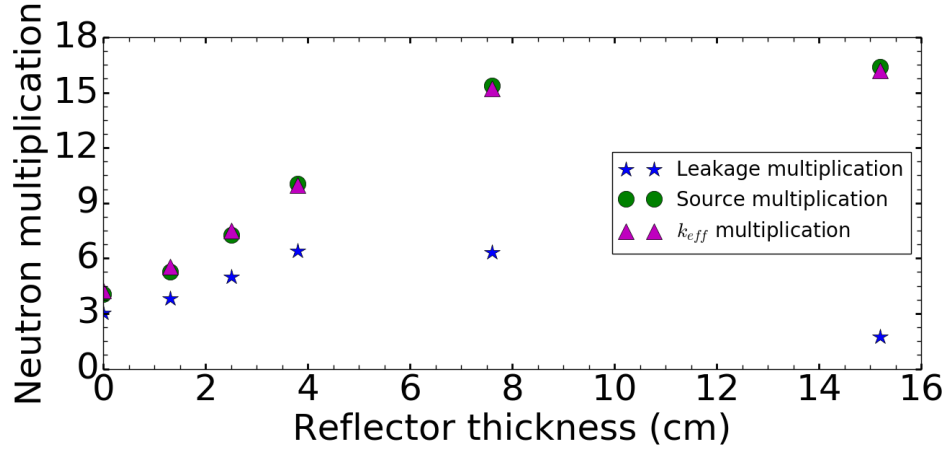


Figure 6: Source, k_{eff} , and leakage multiplication as a function of polyethylene reflector thickness.

Leakage multiplication is defined in terms of the neutron leakage and therefore follows a trend similar to that of Y as a function of reflector thickness. The source and k_{eff} multiplication monotonically increase as a function of reflector thickness because they are defined in terms of neutrons that are within the system and do not depend on neutron leakage. Their values are similar to one another for all polyethylene reflector thicknesses because the Pu-240 spontaneous fission neutron spectrum is similar to the Pu-239 induced fission neutron spectrum.

Figure 7 is a plot of a linear and a quadratic model fit to the simulated Y and Sm_2 as a function of source multiplication. Figures 8, 9, and 10 are analogous plots of Y and Sm_2 as a function of k_{eff} multiplication, leakage multiplication, and polyethylene reflector thickness, respectively. The uncertainty in Y and Sm_2 is again that due to covariance in the cross sections. The fits were performed using the Levenburg-Marquardt algorithm to minimize a chi-squared error metric.

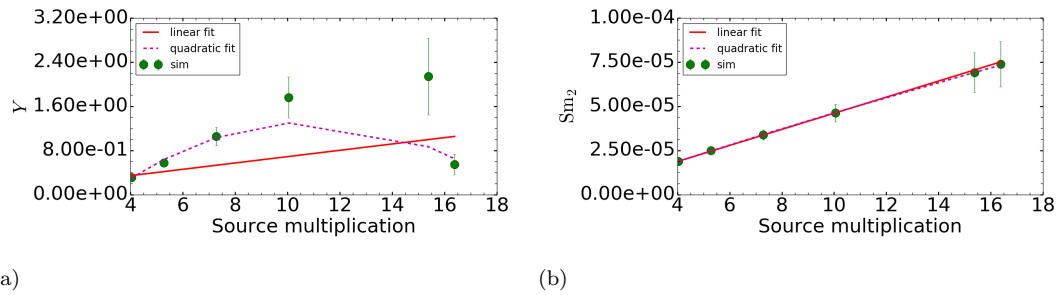


Figure 7: Fit of a linear and quadratic model to the simulated (a) Y and (b) Sm_2 as a function of source multiplication.

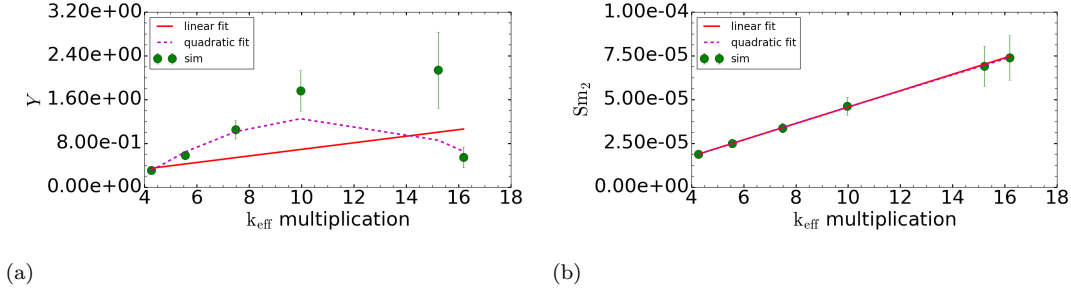


Figure 8: Fit of a linear and quadratic model to the simulated (a) Y and (b) Sm_2 as a function of k_{eff} multiplication.

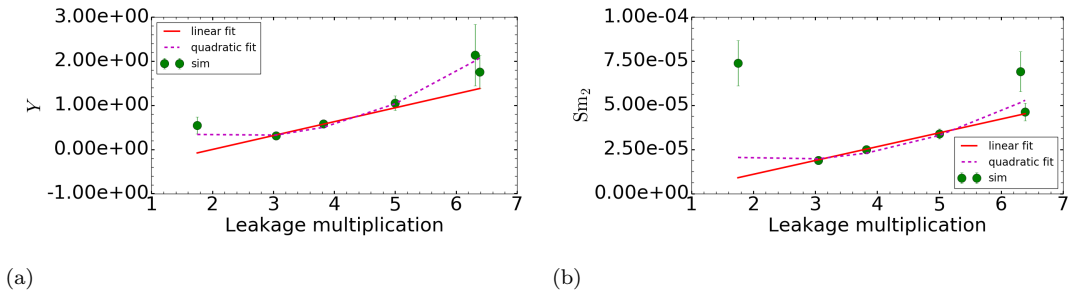


Figure 9: Fit of a linear and quadratic model to the simulated (a) Y and (b) Sm_2 as a function of leakage multiplication.

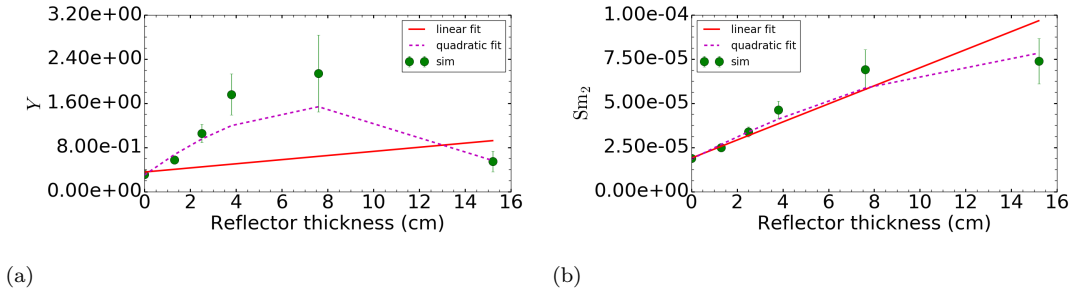


Figure 10: Fit of a linear and quadratic model to the simulated (a) Y and (b) Sm_2 as a function of polyethylene reflector thickness.

There is a linear relationship between Sm_2 and both source and k_{eff} multiplication, and the behavior of Sm_2 as a function of reflector thickness appears to be quadratic. Measurements of Sm_2 may therefore be used to infer specific types of neutron multiplication or reflector thickness. The behavior of Y as a function of neutron multiplication and reflector thickness is not adequately described by the linear or quadratic models, nor is the behavior of Sm_2 as a function of leakage multiplication.

IV Summary and recommendations

I have performed the first calculation of the variance Y and Sm_2 due to covariance in the cross sections using deterministic (PARTISN) calculations of the counting distribution moments and first-order, adjoint-based SA. Sm_2

has less variance due to covariance in the cross sections than Y because of its insensitivity to the detector response function. Despite this, Y analysis may still be preferred because of its historical use in inferring integral quantities of SNM [14, 15, 1, 3, 4]. On the other hand, Sm_2 has a linear relationship with source and k_{eff} multiplication and a quadratic relationship with reflector thickness, making it potentially useful for these integral properties, independent of the choice in detector type and placement with respect to the assembly [5, 6].

Acknowledgments

This material was sponsored in part by the National Nuclear Security Administration (NNSA) Office of Defense Nuclear Nonproliferation R&D through the Consortium for Nonproliferation Enabling Capabilities (CNEC) through grant number DE-NA0002576.

References

- [1] M. Smith-Nelson, K. Butterfield, W. Geist, D. Mayo, E. Shores, B. Rooney, and D. Dinwiddle, “Neutron Specialist Handbook and Informational Text,” 2007. Los Alamos National Laboratory Report LA-UR-07-6170.
- [2] E. C. Miller, J. K. Mattingly, S. D. Clark, C. J. Solomon, B. Dennis, A. Meldrum, and S. A. Pozzi, “Computational Evaluation of Neutron Multiplicity Measurements of Polyethylene-Reflected Plutonium Metal,” *Nucl. Sci. Eng.*, vol. 176, pp. 167–185, 2014. <http://dx.doi.org/10.13182/NSE12-53>.
- [3] J. Mattingly, “Computation of Neutron Multiplicity Statistics using Deterministic Transport,” *IEEE Trans. Nucl. Sci.*, vol. 59, pp. 314–322, April 2012. <https://doi.org/10.1109/NSSMIC.2009.5402335>.
- [4] A. M. Okowita and J. Mattingly, “Analysis of the Feynman Variance to Mean Ratio using Nonlinear Regression,” *INMM 53rd Annual Meeting, Orlando*, 2012.
- [5] M. A. Smith-Nelson and J. D. Hutchinson, “The Sm_2 Ratio for Evaluating Neutron Multiplicity Models,” Nov. 2014. Los Alamos National Laboratory Report LA-UR-07-6170, <https://doi.org/10.2172/1164461>.
- [6] A. McSpaden, M. Nelson, and J. Hutchinson, “Eliminating Detector Response in Neutron Multiplicity Measurements for Model Evaluation,” *Trans. Am. Nucl. Soc., Washington, D.C., Oct. 29-Nov. 2*, vol. 117, 2017.
- [7] T. M. Evans, A. S. Stafford, R. N. Slaybaugh, and K. T. Clarno, “Denovo: A New Three-Dimensional Parallel Discrete Ordinates Code in SCALE,” *Nucl. Tech.*, vol. 171, no. 2, pp. 171–200, 2010. <https://doi.org/10.13182/NT171-171>.
- [8] R. T. Evans, J. K. Mattingly, and D. G. Cacuci, “Sensitivity Analysis and Data Assimilation in a Subcritical Plutonium Metal Benchmark,” *Nucl. Sci. Eng.*, vol. 176, pp. 325–338, 2014. <https://doi.org/10.13182/NES13-24>.
- [9] M. B. Chadwick, “ENDF/B-VII.0: Next Generation Evaluated Nuclear Data Library for Nuclear Science and Technology,” *Nuclear Data Sheets*, vol. 107, no. 12, pp. 2931–3060, 2006. <https://doi.org/10.1016/j.nds.2006.11.001>.
- [10] L. Pål, “On the Theory of Stochastic Processes in Nuclear Reactors,” *Il Nuovo Cimento*, vol. 7, no. 1, pp. 25–42, 1958.
- [11] G. I. Bell, “On the Stochastic Theory of Neutron Transport,” *Nucl. Sci. Eng.*, vol. 21, pp. 390–401, 1965. <https://doi.org/10.13182/NSE65-1>.
- [12] J.-L. Muñoz-Cobo, R. B. Perez, and G. Verdu, “Stochastic Neutron Transport Theory: Neutron Counting Statistics in Nuclear Assemblies,” *Nucl. Sci. Eng.*, vol. 95, no. 2, pp. 83–105, 1987. <https://doi.org/10.13182/NSE95-83>.
- [13] S. O’Brien, J. Mattingly, and D. Anistratov, “Sensitivity Analysis of Neutron Multiplicity Counting Statistics for a Subcritical Plutonium Metal Benchmark using First-Order Perturbation Theory,” *Nucl. Sci. Eng.*, vol. 185, no. 3, pp. 406–425, 2017. <https://doi.org/10.1080/00295639.2016.1272988>.

- [14] R. P. Feynman, F. D. Hoffmann, and R. Serber, “Dispersion of the Neutron Emission in U-235 Fission,” *J. Nucl. Energy*, vol. 3, pp. 64–69, 1956. [https://doi.org/10.1016/0891-3919\(56\)90042-0](https://doi.org/10.1016/0891-3919(56)90042-0).
- [15] A. A. Robba, E. J. Dowdy, and H. F. Atwater, “Neutron Multiplication Measurements using Moments of the Neutron Counting Distribution,” *Nucl. Instrum. Methods.*, vol. 215, pp. 473–479, 1983. [https://doi.org/10.1016/0167-5087\(83\)90481-7](https://doi.org/10.1016/0167-5087(83)90481-7).
- [16] R. E. Alcouffe, R. S. Baker, J. A. Dahl, S. Turner, and R. Ward, “PARTISN: Time-Dependent, Parallel Neutral Particle Transport Code System,” Nov. 2008. Los Alamos National Laboratory Report LA-UR-08-07258.
- [17] J. A. Favorite, “SENSMG: First-Order Sensitivities of Neutron Reaction Rates, Reaction-Rate Ratios, Leakage, k_{eff} , and α Using PARTISN,” *Nucl. Sci. Eng.*, vol. 192, no. 1, pp. 80–114, 2018. <https://doi.org/10.1080/00295639.2018.1471296>.
- [18] J. A. Favorite, Z. Perkó, B. C. Kiedrowsky, and C. M. Perfetti, “Adjoint-Based Sensitivity and Uncertainty Analysis for Density and Composition: A User’s Guide,” *Nucl. Sci. Eng.*, vol. 185, no. 3, pp. 384–405, 2017. <https://doi.org/10.1080/00295639.2016.1272990>.
- [19] *Scale: A Comprehensive Modeling and Simulation Suite for Nuclear Safety Analysis and Design*, ornl/tm-2005/39, version 6.1 ed., June 2011. Available from Radiation Safety Information Computational Center at Oak Ridge National Laboratory as CCC-785.
- [20] J. A. Favorite, “Flux Moments and Inner Products (U),” Nov. 2008. Los Alamos National Laboratory Research Note X-1-RN(U)09-02, (November 25, 2008).
- [21] C. J. Werner, *MCNP User’s Manual, Code Version 6.2.0*, October 2017. Los Alamos National Laboratory Report LA-UR-17-29981.
- [22] S. M. Girard, *MCNP - A General Monte Carlo N-Particle Transport Code, Version 5*, 2003. Los Alamos National Laboratory Report LA-UR-03-1987.

ARC:arc

Distribution:

A. Sood, XCP-3, MS F663, sooda@lanl.gov
J. L. Hill, XCP-3, MS F663, jimhill@lanl.gov
J. A. Favorite, XCP-3, MS F663, fave@lanl.gov
K. C. Bledsoe, Oak Ridge National Laboratory, bledsoekc@ornl.gov
J. D. Hutchinson, NEN-2 MS B228, jesson@lanl.gov
A. T. McSpaden, NEN-2 MS B228, mcspaden@lanl.gov
W. L. Myers, NEN-2 MS B228, bmyers@lanl.gov
M. A. Nelson, NEN-2 MS B228, manelson@lanl.gov
G. J. Dean, XCP-3, MS K784, gjdean@lanl.gov
A. R. Clark, XCP-3, MS P363, arclark@lanl.gov
XCP-3 File
X-Archive, xarchive@lanl.gov

Appendix A Sample PARTISN input decks

This input deck was used to perform a fixed source ($\text{ievt} = 0$), forward ($\text{ith} = 0$) transport solve for the 3.8-cm polyethylene-reflected BeRP ball. The file “xslib” refers to the cross section library generated by the SCALE code package [19]. “chivec” was also obtained from SCALE. The fixed source “sourcf” was computed using a Watt fission spectrum for Pu-240 with parameters $a = 0.794930$ MeV, $b = 4.68927$ MeV⁻¹ (from Appendix C, Table 9.1.2.2 of [21]) and a rate of spontaneous fission neutron emission from Pu-240 in the BeRP ball of 2.78×10^5 $\frac{\text{SF neutrons emitted}}{\text{sec}}$ (Table III of [2]).

```

      1      0      0
fwd_npod_3_collapsed_44
/ BLOCK 1
  igeom=sphere
  isn=256
  ngroup=44
  niso=4
  mt=2
  nzone=2
  im=2
  it=760
  t
/ BLOCK 2
  xmesh=
  0.0
  3.7938
  7.604
  xints=
  379
  381
  zones=
  1
  2
  t
/ BLOCK 3
  lib=xslib
  i2lp1= 1
  ititl= 1
  names="c", "pu-239", "pu-240", "h-poly"
  maxord= 5
  ihm= 74
  iht= 9
  ihs= 31
  ifido= 2
  savbxs= 0
  chivec=
  7.8298399999999994e-03
  1.8158700000000000e-02
  5.0958200000000002e-02
  1.6236200000000001e-01
  8.7765200000000002e-02
  2.4851700000000001e-02
  1.1633200000000000e-01
  1.2526100000000001e-01
  1.5820999999999999e-01
  1.6231599999999999e-01
  7.4411000000000005e-02

```

```
1.0074600000000000e-02
6.4720299999999995e-04
7.7167999999999996e-04
5.1216199999999999e-05
4.3478500000000001e-08
1.3526600000000000e-09
1.1891600000000001e-10
5.1118999999999997e-12
4.4013400000000003e-12
1.9974100000000001e-12
2.0159900000000002e-12
8.7211099999999998e-13
3.1704400000000002e-13
9.0580200000000006e-14
3.4281099999999998e-14
2.8799900000000001e-15
2.6941799999999999e-15
2.5083700000000002e-15
4.4593299999999998e-15
0.0000000000000000e+00
0.0000000000000000e+00
0.0000000000000000e+00
0.0000000000000000e+00
0.0000000000000000e+00
0.0000000000000000e+00
0.0000000000000000e+00
0.0000000000000000e+00
0.0000000000000000e+00
0.0000000000000000e+00
0.0000000000000000e+00
0.0000000000000000e+00
0.0000000000000000e+00
0.0000000000000000e+00
0.0000000000000000e+00
0.0000000000000000e+00
0.0000000000000000e+00
t
/ BLOCK 4
matls=
  m1
pu-239 0.0460595191156
pu-240 0.00290503749976
;
  m2
h-poly 0.0809882249
c 0.0404015978
;
assign=
zone1 m1 1.0 ;
zone2 m2 1.0 ;
t
/ BLOCK 5
ievt=0
isct=5
epsi= 1.00E-06
iitm=999
srcacc=no
npeg=2
avatar=1
raflux=1 rmflux=1
```

```
xsectp=2
ith=0
iitl=0
oitm=9999
sourcf=
379r 3.2183315687538063e+00 381r 0.0 ;
379r 1.1986607422794732e+01 381r 0.0 ;
379r 4.4331060606044495e+01 381r 0.0 ;
379r 1.7852172035076097e+02 381r 0.0 ;
379r 1.0520053508284677e+02 381r 0.0 ;
379r 3.1693082875545414e+01 381r 0.0 ;
379r 1.4435263000478150e+02 381r 0.0 ;
379r 1.6124776107669450e+02 381r 0.0 ;
379r 2.0816401111097369e+02 381r 0.0 ;
379r 2.1279278916978717e+02 381r 0.0 ;
379r 9.8324123632633686e+01 381r 0.0 ;
379r 1.3611771588377923e+01 381r 0.0 ;
379r 8.7320081608675915e-01 381r 0.0 ;
379r 1.0371608984499858e+00 381r 0.0 ;
379r 7.6852703925508956e-02 381r 0.0 ;
379r 6.0437195244846210e-03 381r 0.0 ;
379r 4.2452903812439377e-04 381r 0.0 ;
379r 6.7410380091630675e-05 381r 0.0 ;
379r 4.3535872405907212e-06 381r 0.0 ;
379r 4.2450246637305983e-06 381r 0.0 ;
379r 2.2071094399002550e-06 381r 0.0 ;
379r 2.6194585207126969e-06 381r 0.0 ;
379r 1.4434427880193511e-06 381r 0.0 ;
379r 6.8827966914412380e-07 381r 0.0 ;
379r 2.5700365218059759e-07 381r 0.0 ;
379r 1.2249534292605695e-07 381r 0.0 ;
379r 1.1858453190838746e-08 381r 0.0 ;
379r 1.1469474304884600e-08 381r 0.0 ;
379r 1.1066826302061150e-08 381r 0.0 ;
379r 2.0862954895162132e-08 381r 0.0 ;
379r 9.7596591725520346e-09 381r 0.0 ;
379r 9.2830931208539340e-09 381r 0.0 ;
379r 8.7806742932256685e-09 381r 0.0 ;
379r 1.5925358136448806e-08 381r 0.0 ;
379r 1.3448261074539758e-08 381r 0.0 ;
379r 6.6563257113148412e-09 381r 0.0 ;
379r 3.7288173327726083e-09 381r 0.0 ;
379r 1.6156726135457400e-09 381r 0.0 ;
379r 1.4244074296968286e-09 381r 0.0 ;
379r 5.9536816077276945e-10 381r 0.0 ;
379r 1.5363563937478885e-09 381r 0.0 ;
379r 1.7805093094643969e-10 381r 0.0 ;
379r 2.4649191199752855e-10 381r 0.0 ;
379r 8.3459943427857428e-11 381r 0.0 ;
t
```

This input deck was used to perform a fixed source ($ievt = 0$), adjoint ($ith = 1$) transport solve for the 3.8-cm polyethylene-reflected BeRP ball. The cross sections and fission spectrum were also generated by SCALE [19]. The adjoint right-boundary source “sirite” is the detector response function for the nPod neutron multiplicity counter in units of $\frac{\text{counts}}{\text{leakage neutron}}$ and was generated by Mattingly using MCNP5[®] [22].

```
      1      0      0
adj_inpod_3_collapsed_44
/ BLOCK 1
  igeom=sphere
  isn=256
  ngroup=44
  niso=4
  mt=2
  nzone=2
  im=2
  it=760
  t
/ BLOCK 2
  xmesh=
  0.0
  3.7938
  7.604
  xints=
  379
  381
  zones=
  1
  2
  t
/ BLOCK 3
  lib=xslib
  i2lp1= 1
  ititl= 1
  names="c", "pu-239", "pu-240", "h-poly"
  maxord= 5
  ihm= 74
  iht= 9
  ihs= 31
  ifido= 2
  savbxs= 0
  chivec=
  7.8298399999999994e-03
  1.8158700000000000e-02
  5.0958200000000002e-02
  1.6236200000000001e-01
  8.7765200000000002e-02
  2.4851700000000001e-02
  1.1633200000000000e-01
  1.2526100000000001e-01
  1.5820999999999999e-01
  1.6231599999999999e-01
  7.4411000000000005e-02
  1.0074600000000000e-02
  6.4720299999999995e-04
  7.7167999999999996e-04
  5.1216199999999999e-05
  4.3478500000000001e-08
```

```

1.3526600000000000e-09
1.1891600000000000e-10
5.1118999999999997e-12
4.4013400000000000e-12
1.9974100000000000e-12
2.0159900000000000e-12
8.7211099999999998e-13
3.1704400000000000e-13
9.0580200000000000e-14
3.4281099999999998e-14
2.8799900000000000e-15
2.6941799999999999e-15
2.5083700000000000e-15
4.4593299999999998e-15
0.0000000000000000e+00
0.0000000000000000e+00
0.0000000000000000e+00
0.0000000000000000e+00
0.0000000000000000e+00
0.0000000000000000e+00
0.0000000000000000e+00
0.0000000000000000e+00
0.0000000000000000e+00
0.0000000000000000e+00
0.0000000000000000e+00
0.0000000000000000e+00
0.0000000000000000e+00
0.0000000000000000e+00
0.0000000000000000e+00
0.0000000000000000e+00
0.0000000000000000e+00
0.0000000000000000e+00
t
/ BLOCK 4
matls=
    m1
pu-239 0.0460595191156
pu-240 0.00290503749976
;
    m2
h-poly 0.0809882249
c 0.0404015978
;
assign=
zone1 m1 1.0 ;
zone2 m2 1.0 ;
t
/ BLOCK 5
ievt=0
isct=5
epsi= 1.00E-06
iitm=999
srcacc=no
npeg=2
avatar=1
raflux=1 rmflux=1
xsectp=2
ith=1
iitl=0
oitm=9999
sirite=

```

0.00230160520555
0.00371784656128
0.00459180276459
0.00592534168591
0.00770316452173
0.00770316452173
0.00837828241201
0.00995355748932
0.0102947222336
0.0127035156593
0.0144456041245
0.0153663254116
0.0159139863479
0.0163303213353
0.0173531576995
0.0183219467911
0.0191775098412
0.020221796808
0.0207877673055
0.0208408891122
0.0208935827561
0.0207484659846
0.0203868343663
0.0198786130018
0.0174256527423
0.0111902991251
0.00234293931949
0.00234293931949
0.00234293931949
0.00118844819145
3.39570634051e-05
3.39570634051e-05
3.39570634051e-05
2.88770397554e-09
2.88770397554e-09
1.0269997652e-07
7.35069746499e-07
1.11887634574e-06
9.11283166745e-07
6.27019257584e-07
2.84650314559e-07
5.10684875829e-09
4.44314322532e-09
1.30644952429e-10
t
/ BLOCK 6
pted=0 zned=0 ajed=0
t